Hydrogenation of Dimethyl Oxalate to Ethylene Glycol on a Cu/SiO_2/Cordierite Monolithic Catalyst: Enhanced Internal Mass Transfer and Stability

Hairong Yue, Yujun Zhao, Li Zhao, Jing Lv, Shengping Wang and Jinlong Gong, and Xinbin Ma
Key Laboratory for Green Chemical Technology of Ministry of Education, School of Chemical Engineering and Technology, Tianjin University, Tianjin 300072, China

DOI 10.1002/aic.12785
Published online November 2, 2011 in Wiley Online Library (wileyonlinelibrary.com).

The design and application of a Cu/SiO_2-based monolithic catalyst for hydrogenation of dimethyl oxalate (DMO) to ethylene glycol (EG) is presented. The catalyst was dip-coated on cordierite with highly dispersed Cu/SiO_2 slurry prepared by ammonia evaporation method. This structure guarantees high dispersion of copper species within the mesopores of silica matrix in the form of copper phyllosilicate. The catalyst is low cost, stable, and exhibits high activity in the reaction of hydrogenation of DMO, achieving a 100% conversion of DMO and more than 95% selectivity to EG. Notably, STY_{EG} over the monolith is significantly enhanced compared to the packed bed Cu/SiO_2 catalysts in both forms of pellet and cylinder. It is primarily due to the relatively short diffusive pathway of the thin wash-coat layer and high efficiency of the active phase derived from the monolithic catalyst. Theoretical results indicated that the internal mass transfer is dominated on the catalysts of pellet and cylinders. Moreover, the monolithic catalyst possessed excellent thermal stability compared to the pellet catalyst, which is attributed to the regular channel structure, uniform distribution of flow. *AIChE J,* 58: 2798–2809, 2012
Keywords: monolithic catalyst, hydrogenation, dimethyl oxalate, ethylene glycol, internal diffusion

Introduction

Ethylene glycol (EG) is an important chemical used in a variety of industrial applications. Recognized uses of EG are in the areas of antifreeze,[1] polyester fiber, and polyester resins, as well as the manufacture of asphalt emulsion paints, heats transfer agents, brake fluids and solvents. For the past decade, there has been an increasing interest in the development of catalyst for reforming of EG to hydrogen[2–4] and electro-oxidation of EG to alcohol fuel cells.[5] At present, ethylene oxidation is a universal industrial process to produce EG. However, as a result of the depletion of petroleum resource as well as the constantly increased demand of EG,[6,7] synthesis of EG from syngas (e.g., derived from coal, natural gas, and biomass) has become considerably significant and attracted numerous interests. The indirect synthetic process includes the coupling of CO with methanol (to form dimethyl oxalate (DMO)) and subsequent hydrogenation to EG.[8,9] While a number of investigations have been reported on the first reaction, this article focuses on the design and utilization of monolithic catalysts for hydrogenation of DMO to EG.

Selective catalytic hydrogenation of DMO involves several reactions. The reaction (i) is the first step of hydrogenation of DMO, in which intermediate methyl glycolate (MG) is formed

$$CH_3OOCCOOCH_3 + 2H_2 \rightarrow CH_3OOCCH_2OH + CH_3OH \qquad \Delta H = -30.03\,kJ/mol \quad (i)$$

The followed reaction (ii) is hydrogenation of MG to target product EG

$$CH_3OOCCH_2OH + 2H_2 \rightarrow HOCH_2CH_2OH + CH_3OH \qquad \Delta H = -28.70\,kJ/mol \quad (ii)$$

Along with main reactions, a couple of side reactions also occur. EG can be deeply hydrogenated to ethanol, and the formed ethanol reacts with EG leading to the formation of 1, 2-butanediol (1, 2-BDO)

$$HOCH_2CH_2OH + H_2 \rightarrow C_2H_5OH + H_2O \qquad \Delta H = -87.20\,kJ/mol \quad (iii)$$

$$HOCH_2CH_2OH + C_2H_5OH \rightarrow HOCH_2CH(OH)CH_2CH_3 + H_2O \qquad \Delta H = -61.17\,kJ/mol \quad (iv)$$

The overall reaction for synthesis of EG is shown as follow

$$CH_3OOCCOOCH_3 + 4H_2 \rightarrow HOCH_2CH_2OH + 2CH_3OH \qquad \Delta H = -58.73\,kJ/mol \quad (v)$$

Hydrogenation of DMO has been previously carried out in both homogeneous and heterogeneous systems based on

Correspondence concerning this article should be addressed to X. Ma at xbma@tju.edu.cn.

noble-metal catalysts, such as Ru[10–12] and Ag.[13] However, these homogeneous catalysts are expensive and suffer from separation issue.[7,14] Therefore, developments of inexpensive catalysts have attracted increased attention recently.[7,13–17] Among them, copper-based catalysts are active for vapor-phase hydrogenation of oxalates to EG.[18–20] Copper sites are considered to be active for the selective hydrogenation of carbon-oxygen bonds and relatively inactive for the hydrogenolysis of carbon-carbon bonds.[18] Different carriers (e.g., SiO_2, Al_2O_3, ZnO, and La_2O_3) for Cu-based catalysts were studied,[21–23] among which Cu/SiO_2 catalysts afforded the highest yield of EG in both hydrogenation of DMO[22] and diethyl oxalate[23] due to weak acidic and basic properties of SiO_2. Recently, mesoporous materials such as hexagonal mesoporous silica (HMS)[14,16,17,24] and SBA[25] have been used as supports for the reaction. It has been reported that strong acidic sites induce the intermolecular dehydration of EG to ethanol, whereas strong basic sites catalyze the Guerbet reaction leading to the formation of 1, 2-BDO.[26] Both products diminish the selectivity to EG. Various synthetic techniques, such as ammonia evaporation (AE), ion exchange, sol–gel, deposition precipitation, and impregnation have been used to fabricate silica-supported copper catalysts.[7,15,25] Notably, the AE method could effectively disperse copper species on the supports (e.g., silica).

Compared with the traditional packed-bed reactor, the monolithic catalyst has several inherent advantages such as high-transport rates of heat and mass per unit pressure drop, high surface area to volume ratios, small transverse temperature gradients and ease of scale-up.[27–29] It has been widely used in treating the exhaust from gasoline powered vehicles, catalytic oxidation of VOCs, removal of NO_x from lean burn and diesel engines, power plant, and furnace exhaust gases for the last two decades.[30–33] The monolith reactor consists of a large number of long, narrow channels in parallel through which reacting fluid flows and the catalyst is deposited in the form of thin wash-coat on the monolith channel wall.[29,34–36] Furthermore, they are commercially available and can resist high temperatures, and the process of coating with catalyst layer is technological developed.[37] Catalyst pellets (e.g., 40–60 mesh) have shown a high activity, but suffer from the problems of catalyst strength and pressure drop over the catalyst bed. Likewise, extruded $\phi 2 \times 2$ and $\phi 3 \times 3$ mm cylindrical catalysts alleviated the problem caused by pressure drop and enhanced the catalyst strength, but they exhibited a lower activity because of diffusion limitation. Thus, monolithic catalysts have been employed to reduce the influence of internal diffusion and radically solve the contradiction between the granular sizes and bed resistance.

Here, we develop a method, directly uploading Cu/SiO_2 catalyst on the cordierite monolith, to prepare a $Cu\text{-}SiO_2$/Cordierite monolithic catalyst for synthesis of EG. The Cu/SiO_2 catalyst powder was prepared by the ammonia evaporation method and dispersed in solvent to form slurry. Subsequently, cordierite monoliths were dip-coated in the Cu/SiO_2 slurry, followed by drying and calcination. This monolith catalyst has been thoroughly characterized by TEM, XRD, N_2 physisorption and TPR, and tested in a continuous monolithic fixed bed reactor under realistic conditions as a function of reaction temperature, space velocity, and thickness of coating layer. We have compared the behavior of the catalysts by varying the configuration (i.e., monolith or packed beds), and experimental conditions such as space velocity. The internal diffusions of the monolith, pellet, and cylinder catalysts have been calculated using a criterion of Wheeler-Weisz group[38,39] to value the internal diffusion effect.[40,41] In addition, the thermal stability of these catalysts was also investigated in reaction conditions.

Experimental

Catalyst preparation

Cylindrical cordierite monoliths (acquired from Corning; 15 mm dia., square channels, 45 mm length, 400 channels per square inch (CPSI)) were wash-coated with catalyst layer by the dip-coating method. Specifically, the slurry was prepared from catalyst powder and deionized water with a weight ratio of 3:5. After wet-milling of the catalyst powder for 10 h, the dried monolith was dipped into the slurry for a few minutes until all air bubbles inside the channels were removed. Subsequently, the monolith was withdrawn from the slurry and the residual liquid inside the channels was removed by flushing thoroughly with pressurized air and then dried at room temperature for 24 h. Upon dryness, the procedure was repeated until the proper loading was achieved. Finally, the monolith was calcined in air at a rate of 5 K/min up to 673 K, and this temperature is kept for 4 h to obtain the Cu/SiO_2 monolith catalysts. The prepared monolith weighed 3.4 ~5.3 g, and the wash-coat content amounted to 7–40 wt % of the monolith weight. The copper content was analyzed by inductive coupled plasma optical emission spectroscopy (ICP-OES) after digestion of the samples in HNO_3 aqueous solutions. In all cases, the copper loading was ~20 wt % with respect to wash-coat and ~1.0–8.0 wt % to the monolith. The experimental uncertainties are estimated to be ~5%.

Cu/SiO_2 powder was prepared by the AE method described briefly as follows. A certain amount of $Cu(NO_3)_2{\cdot}3H_2O$ and 25 wt % ammonia aqueous solution dissolved in deionized water were mixed and stirred for 10 min. Silica sol was then added to the copper ammonia complex solution and stirred for 6 h. The initial pH of the suspension was 11–12. All the aforementioned operations were performed at room temperature. The suspension was heated in a water bath preheated to 353 K to allow for the evaporation of ammonia, the decrease of pH, and the consequent deposition of copper species on silica. When the pH value of the suspension decreased to 6-7, the evaporation process was terminated. The filtrate was washed with deionized water three times, and dried at 393 K for 4 h to obtain the catalyst powder.

Pellet (40–60 mesh, size 250–350 μm) and cylindrical ($\phi 2 \times 2$ mm and $\phi 3 \times 3$ mm) Cu/SiO_2 catalysts were prepared by pressing or extrusion. The catalyst powder was calcined in static air at 673 K for 4 h, pressed, crushed, and sieved or extruded to the desirable size. The obtained monolithic and molded samples were denoted as CuSi/monolith, CuSi/40–60, ϕ2CuSi/cylinder, and ϕ3CuSi/cylinder, respectively.

Catalytic activity tests

Our catalytic reactivity system (monolithic fixed-bed MRCS8004B System) (shown in Figure 1) consists of a continuous-flow stainless steel reactor (15 mm i.d. and 350 mm length) inside a horizontal furnace with a temperature controller. The gas distributor has been equipped at the entrance of the reactor to ensure a uniform gas distribution. The monolithic Cu/SiO_2 catalysts were placed in the middle of the

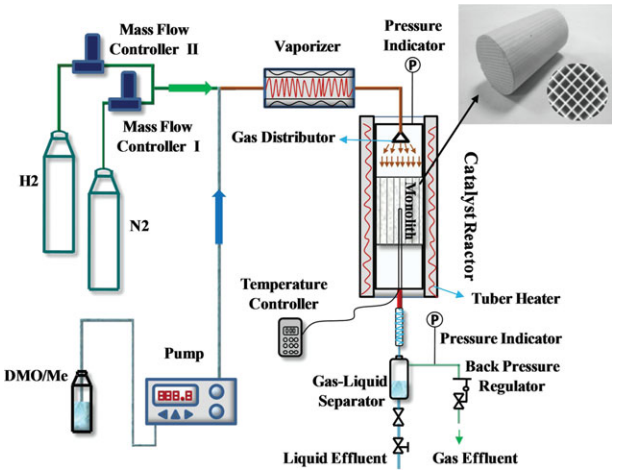

Figure 1. Monolith structure and the monolith reactor flow setup of MRCS8004B system.

[Color figure can be viewed in the online issue, which is available at wileyonlinelibrary.com.]

tube and tightly fitted to the wall of the stainless steel reactor to avoid channeling. The reaction testing was carried out upon the reduction of catalyst in hydrogen atmosphere at 623 K for 4 h. The reactant (20 wt % DMO (99.9% purity) in methanol (AR purity) solution) was injected from the top of the reactor through a high-pressure pump (LabAlliance Series II pump) with a system pressure of 2.5 MPa. Catalytic performance was tested at 473 K. For comparing with the monolithic and molded catalysts, the liquid hourly space velocity (LHSV) of DMO was varied from 0 to 20.3 g_{DMO} g_{Cu}^{-1} h^{-1}(for short h^{-1}). The reaction products were condensed and analyzed on an Agilent Micro GC 6820 with an HP-INNOWAX capillary column (Hewlett-Packard Co., 30 m×0.32 mm×0.50 μm) equipped with a flame ionization detector (FID). Main byproducts include ethanol, methyl glycollate, and 1, 2-butanediol. To ensure repeatability, 4-8 separate GC samples were taken and the results were averaged for each experimental data point, and uncertainties were typically within 3%.

Additionally, for comparison purpose, the monolithic catalyst was crushed and sieved to pellet size (200 um <size <350 um), named crushed CuSi/Monolith. The pellets were diluted and packed (e.g., with a height of 45 mm) in a fixed bed reactor with the same diameter as that used for the monoliths (15 mm i.d). The catalytic packed bed was tested under the same reaction condition as that of the structured catalyst to determine the role of geometrical configuration of the catalyst.

The CuSi/40–60, ϕ2CuSi/Cylinder and ϕ3CuSi/Cylinder catalysts were also tested in a fixed-bed reactor. To keep the same bed height with respect to the crushed monolith, these catalysts were mixed with quartz sand pellets, which is inert for hydrogenation of DMO.

Stability measurements of catalyst were evaluated via the comparison of reactivity of as-prepared catalyst (e.g., 473 K) and that upon thermal treatment (e.g., 623 K) at a DMO LHSV of 10.0 h^{-1}.

Catalyst characterization

Textual properties of the catalysts were determined by nitrogen adsorption method following the ASTM-4365 standard using a Micromeritics Tristar II 3000 analyzer instrument at the boiling temperature of liquid nitrogen. Before analysis, the samples were degassed at 573 K for 4 h *in vacuo*. Pore-size distribution was estimated by the Barrett-Joyner-Halenda (BJH) method from the desorption branches of the adsorption isotherms, and the specific surface areas were calculated from the isotherms using the BET method. Mercury intrusion porosimetry (MIP) tests (Autopore IV, Micromeritics) was used to characterize porosities and tortuosity factor of the calcined catalysts. The expression for calculating the tortuosity factor (derived by Carniglia[42] using Fick's first law of diffusion) is calculated directly from equation $\tau = (2.23 - 1.13V_{tot}\rho_b)(0.92(\frac{4}{S}\sum\frac{\square V_i}{d_i})^{1+\varepsilon})$. It is related to the total pore volume (V_{tot}), bulk density (ρ_b), BET surface area (S), changes in pore volume within a pore-size interval (ΔV_i), average diameter within a pore-size interval (d_i), and pore-shape exponent (ϵ).

The morphology of the monolithic catalysts cut along the profile was examined by a Philips XL-30 scanning electron microscopy (SEM) at 20.0 kV. A Polaron SC500 ion sputtering gun was used for deposition of gold film with thickness of 250 Å onto the samples to enhance electric conductivity. Transmission electron microscopy (TEM) images were obtained using a Philips TECNAI G2 F20 system electron microscope at 100 kV equipped with a field emission gun. The sample powder retrieved from the CuSi/40–60 and the wash-coat of CuSi/monolith was dispersed in ethanol by ultrasonic. Drops of the suspension were applied onto a copper grid-supported transparent carbon foil and dried in air.

TPR was carried out on a Micromeritics Autochem II 2910. Catalyst of 100 mg was loaded into a quartz tube and dried in an argon stream at 393 K for 1 h before the reduction. The catalyst was then heated in 30 mL/min of 5% H_2-Ar at a heating rate of 10 K/min up to 1073 K. A thermal conductivity detector (TCD) was employed to determine the amount of hydrogen consumption during the run.

The specific surface area of metallic copper was measured by the adsorption and decomposition of N_2O using the pulse titration method described in the literature.[15,43] Briefly, 100 mg of catalyst sample was reduced in 5% H_2-Ar at 623 K for 4 h and cooled to 363 K. Then 15%N_2O-Ar was introduced at a rate of 30 mL/min for 2 h, ensuring that surface Cu atoms were completely oxidized according to the reaction $2Cu(s) + N_2O \rightarrow Cu_2O(s) + N_2$. The quantity of chemisorbed N_2O was measured by a hydrogen pulse chromatographic technique on a Micromeritics Autochem II 2910 equipped with a TCD. Hydrogen pulse reduction of surface Cu_2O to metallic copper was conducted at 623 K to ensure that the chemisorbed N_2O on the copper surface immediately reacted with hydrogen gas introduced from the pulse loop. Hydrogen pulse-dosing was repeated until the pulse area no longer changed. The consumed amount of hydrogen was the value obtained by subtracting the small area of the first few pulses from the area of the other pulses. The specific area of metallic copper was calculated from the total amount of hydrogen consumption with 1.46×10^{19} copper atoms per m^2.[16,44]

XRD measurements were performed using a Rigaku C/max-2500 diffractometer employing the graphite filtered Cu Kα radiation ($\lambda = 1.5406$ Å) at room temperature. The particle size of copper was calculated by X-ray broadening technique using the Scherrer's equation. Data points were acquired by step scanning with a rate of 12°/min from $2\theta = 10°$ to $2\theta = 90°$.

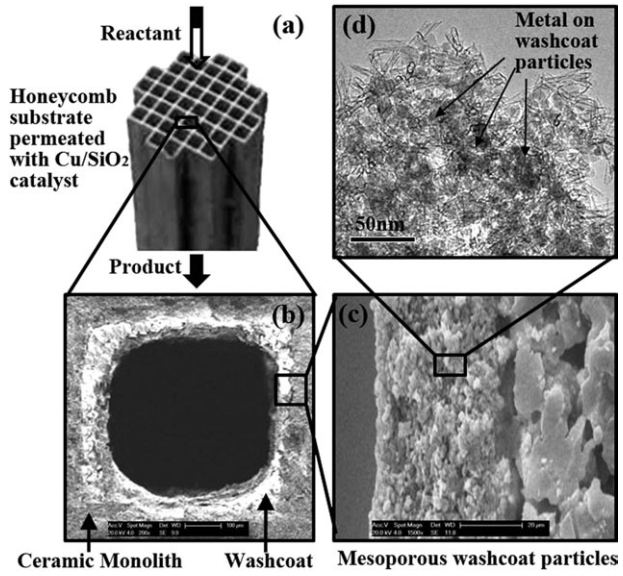

Figure 2. Illustration and morphology of CuSi/Monolith catalyst.

(a) scheme of monolith catalyst, (b) SEM images of a monolith channel, and (c) cross-sectional cordierite monolith wash-coated with Cu/SiO2 catalyst, and (d) TEM image of calcined wash-coat layer.

Mass-transfer calculation

In order to determine the effect of mass transfer with different pellet/cylinder sizes and/or wash-coat thickness, it is essential to estimate the internal mass-transfer resistance. Reaction engineering parameters have been studied for the mass-transfer effects during the reaction regarding external (solid interface) and internal diffusions (pore) using the Carberry number[45] and Wheeler-Weisz[38,39] (W-W) group ($\eta\phi^2$).

The absence of the external mass transfer cannot be ruled out experimentally, but it can be evaluated using Carberry number (Ca),[41,45,46] which is the ratio of observed reaction rate (r_{obs}, mol s^{-1} $g_{\text{cat}}{}^{-1}$) to maximum mass-transfer rate ($r_{\max,i}$)

$$Ca_{gs} = \frac{r_{obs}}{r_{\max,i}} = \frac{r_{obs}}{k_g a_s (C_i^* - C_i^0)} \tag{1}$$

Where k_g is the gas–solid mass-transfer coefficient with a unit of $m_g{}^3$ $m_S{}^{-2}$ s^{-1}; a_S is the external catalyst specific surface area, m^2 g^{-1}; and C_i^* is the bulk concentration of a reactant or product, mol m^{-3}.When the value of the Carberry number is less than 0.05, the reaction is not limited by the external gas–solid mass transfer and the effect of the external mass transfer of the reactant on the reaction rate can be neglected.[41,47,48]

Most mass-transfer correlations in the literature are reported in terms of the Colburn J factor (i.e., J_D) as a function of the Reynolds number ($\text{Re} = \rho_g\, uR/\mu$ = 65–90), and the Schmidt number ($Sc = \mu/\rho_g D_{B,i}$).[49] Both *Re* and *Sc* are relative with the linear velocity u (0.005–0.02 m s^{-1}), and the viscosity (ρ_g) of gases

$$k_g = \frac{D_{Bi}}{R} Sc^{1/3}\, \text{Re} J_D \tag{2}$$

Dwidevi and Upadhyay reviewed a number of mass-transfer correlations for both fixed and fluidized beds and arrived at the following correlation, which is valid for gases (*Re* >10) in either fixed or fluidized.[50,51] The relationship between J_D and the Reynolds numbers is

$$J_D = \frac{1}{\theta}\left(\frac{0.765}{\text{Re}^{0.82}} + \frac{0.365}{\text{Re}^{0.386}}\right) \tag{3}$$

The W-W group has been reported[41,47,52–54] to investigate the influence of internal diffusion. When the value of $\eta\phi^2$ is less than 0.1, the effect of the internal mass transfer of the reactant on the reaction rate can be neglected.[55,56] Here, we calculate the internal mass-transfer parameters of the monolith catalyst to examine the internal diffusions and its influence. The W-W group is defined as follows

$$\eta\varphi^2 = \frac{\boldsymbol{r_{obs} R^2}}{\boldsymbol{D_{eff,i} C_i^*}} \tag{4}$$

R represents the diameter of pellet and cylindrical catalysts.[40,41] For the monolithic catalyst, the thin coating of Cu/SiO_2 catalyst on the wall of cordierite square monolith channels, observed by SEM in Figure 2, is considered to be slabs. Therefore, R represents the thickness of the coating layer (estimation using scanning electron microscopy) for the monolithic catalyst.[41] The parallel pore model proposed by Wheeler is a general relationship between the effective diffusivity ($D_{eff,i}$), and the pore diffusivity (D_P) via the porosity of the solid[38]

$$\boldsymbol{D_{eff,i} = \frac{\varepsilon}{\tau} D_p} \tag{5}$$

Where ϵ is the porosity and τ is the tortuosity factors, which can be measured by BET method and mercury porosimeter, respectively. The diffusion coefficient (D_P) in the pores can be determined as a combination of the Knudsen diffusion coefficient (D_K) and the bulk diffusion coefficient ($D_{B,i}$).[40] For equimolar counter diffusion, the two diffusivities can be combined using the Bosanquet formula[57] to give the diffusion coefficient in the pore.

$$\boldsymbol{\frac{1}{D_P} = \frac{1}{D_K} + \frac{1}{D_{B,i}}} \tag{6}$$

The Knudsen diffusion coefficient depends on temperature, molar mass of the diffusing species, and pore dia. (d_p)[29]

$$\boldsymbol{D_K = 48.5 d_p \sqrt{\frac{T}{M_i}}} \tag{7}$$

The bulk diffusion coefficient for a multicomponent mixture can be computed from, for example, the relationship proposed by Poling et al.[58]

$$\boldsymbol{\frac{1}{D_{B,i}} = \frac{1}{1 - y_i} \sum_{j=2}^{n} \frac{y_i}{D_{ij}}} \tag{8}$$

$$\boldsymbol{D_{ij} = \frac{1 \times 10^{-3} T^{3/2}}{P\left[(\sum V)_i^{1/3} + (\sum V)_i^{1/3}\right]^2} \left[\frac{1}{M_i} + \frac{1}{M_j}\right]^{1/2}} \tag{9}$$

For the nonideal properties of the materials in practice, the average pore size, porosity, and tortuosity factor need to

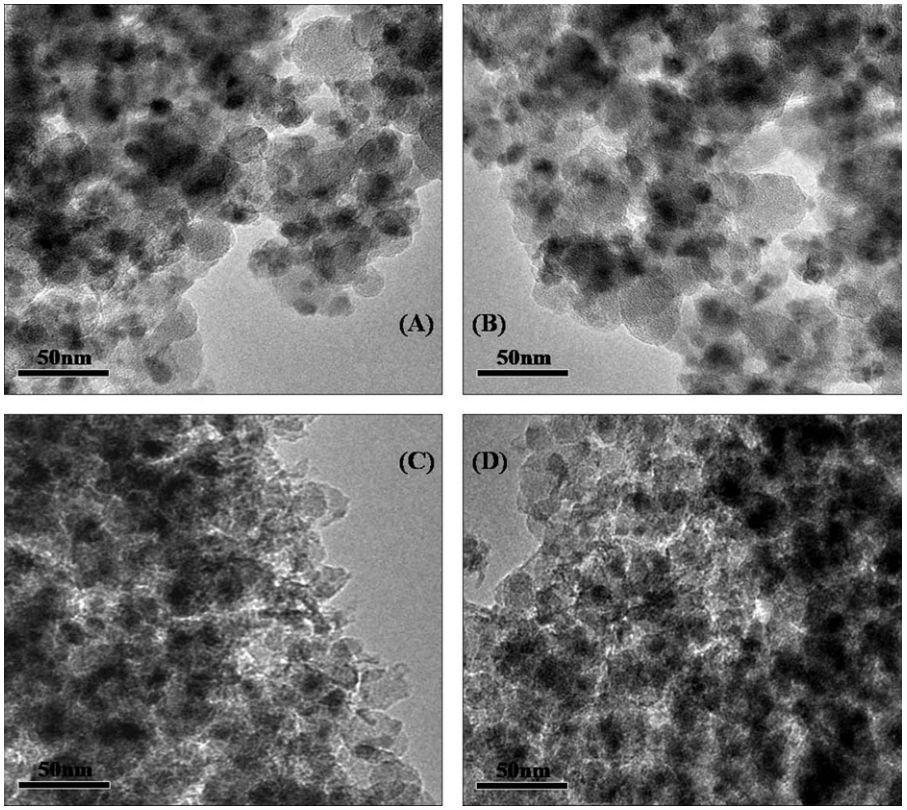

Figure 3. TEM images of the reduced and used CuSi/40–60 and CuSi/Monolith samples: (A) Reduced CuSi/Monolith; (B) Reduced CuSi/40–60; (C) Used CuSi/Monolith; (D) Used CuSi/40–60.

(The used is after stability experiment).

be determined experimentally. Therefore, the mean values of pore diameter and tortuosity factor were used for the effective diffusivity calculation.

Results

Morphology

Textural characteristics of wash-coated CuSi/Monolith catalysts were observed by SEM, as shown in Figure 2. The monolithic catalyst consists of honeycomb monolith channels whose walls were covered with a thin coating of porous Cu/SiO_2 catalyst (Figure 2b), which was dip-coated on the surface of the cordierite monolith with a certain thickness (Figure 2c).

TEM image for the wash-coat of the calcined CuSi/Monolith catalyst (Figure 2d) indicated that small copper nanoparticles were well-dispersed in the SiO_2 matrix. Figure 3A and 3B are TEM images of reduced and used samples of CuSi/monolith and CuSi/40–60 samples. The black spherical particles attributed to Cu species demonstrated that the morphology of copper phyllosilicate disappeared to some extent after reduction.[7] The Cu nanoparticles remained small after reduction and were not easily observed with regular shape in both reduced CuSi/monolith and CuSi/40–60 samples. However, in the TEM images of the used CuSi/monolith (Figure 3C) and CuSi/40–60 (Figure 3D) catalysts, the copper species agglomerated to large particles compared to the reduced samples.

Textural properties

Figure 4 shows the pore-size distribution (PSD) curves of CuSi/monolith, CuSi/40–60, and ϕ2CuSi/cylinder catalysts. Isotherms of the catalysts are also displayed for comparison. BET surface area, pore volume, and average pore diameter were summarized in Table 1. All three catalysts have comparable surface areas and pore diameter. The narrow PSD curves derived from desorption branch show that pores at about 2.0 and 10.0 nm are major contributors to the total pore volume. The mean pore size of CuSi/monolith catalyst changed slightly from 7.2 nm to 7.4 nm compared to the CuSi/40–60 catalyst. Additionally, the BET specific surface

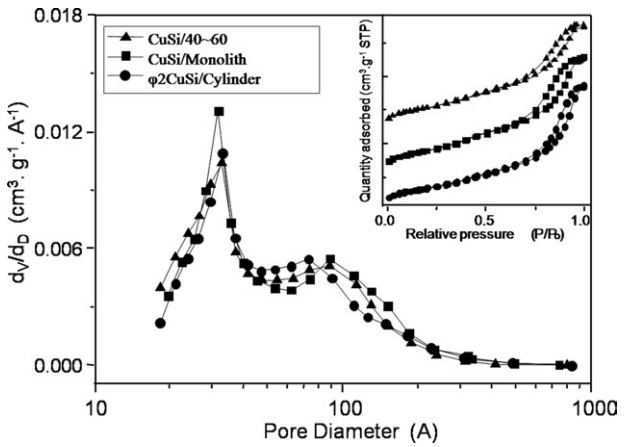

Figure 4. Pore-size distribution of CuSi/monolith (■), ϕ2CuSi/Cylinder (●), and CuSi/40–60 (▲), calculated applying the BJH method to the desorption isotherm.

The inset shows the N_2 adsorption/desorption isotherms.

Table 1. Textural Parameters of CuSi/Monolith, CuSi/40–60, and ϕ2CuSi/Cylinder Catalysts

Catalyst	Surface Area (m^2/g)	Mean pore diameter[a] (nm)	Cu loading (%)	Cu dispersion %	$Cu^0/(Cu^0+Cu^I)$	S_{Cu}[e] $m^2\ g^{-1}$	Tortuosity factor[d]
CuSi/40~60	483	7.2	19.3%	20.7	0.21	25.8	1.41
CuSi/Monolith[b]	502	7.4	19.0% (7.0%)[c]	20.5	0.21	25.6	1.37
ϕ2CuSi/Cylinder	387	6.3	19.3%	19.3	0.20	24.1	1.63
ϕ3CuSi/Cylinder	389	6.0	19.3	17.2	0.18	21.2	1.72

[a] Determined by BJH pore size distribution of N_2 adsorption.
[b] The textural parameters of CuSi/Monolith based on the catalyst wash-coat layer (thickness of 35 μm).
[c] Cu on the wash-coat layer and monolithic catalyst is 19.0% and about7.0%, respectively; the bare cordierite does not contain Cu.
[d] Measured by mercury porosimeter.
[e] Determined by N_2O surface oxidation; S_{Cu}: metallic surface area.

area (502 $m^2 \cdot g^{-1}$) and pore volume (0.93 $cm^3 \cdot g^{-1}$) enlarged slightly for the CuSi/monolith catalyst, which may be due to the smaller and sphere ball-milled catalyst particles in the wash-coat. Nevertheless, these differences in surface area were not deemed significant considering experimental uncertainties. Therefore, the textural properties of the washcoat on the monolith catalyst remained nearly unchanged upon the ball-milling and coating process.

Figure 4 and Table 1 also show a comparison of the textural parameters of CuSi/Monolith and ϕ2CuSi/cylinder catalysts. The mean pore size of ϕ2CuSi/cylinder was slightly smaller than CuSi/40–60 catalyst, while the BET specific surface area and mean pore diameter decreased to 387 $m^2 \cdot g^{-1}$ and 6.0 nm, respectively. This could be ascribed to the mechanical molding process. The accessible surface copper atoms (determined by N_2O chemisorptions), which contributes mainly the catalytic performance,[16] are comparable on the four types of catalysts. The fraction of Cu^0 (Cu dispersion %) (see Table 1) was found to be lower than $Cu^0/(Cu^+ + Cu^0)$ for all the catalysts. This result indicates that small amounts of CuO species (ca. 3–5%) was wrapped up, and could not be reduced in this condition. The tortuosity factor increased with the pellet/cylinder sizes, suggesting that textural properties of the catalysts become complicated upon extrusion.

TPR measurements were performed to investigate the reducibility of both CuSi/monolith and CuSi/40–60 samples calcined at 623 K (Figure 5). The CuSi/monolith sample displayed a sharp reduction peak centered at 558 K, while the CuSi/40–60 catalyst showed a higher reduction temperature. The copper in the structure of copper phyllosilicate is hard to be reduced.[7,59] Highly dispersed copper species on silica supports have been well documented to be more readily reduced than bulk cupric oxide.[15] The lower reduction temperature of CuSi/monolith with respect to the CuSi/40–60 catalyst is probably due to relatively weak interaction between Cu and SiO_2, or the Cu species in the wash-coat relatively weakly bound with hydrogen. In addition, the reduction profiles of both catalysts are sharp and almost symmetrical, indicating a narrow distribution of particle size.

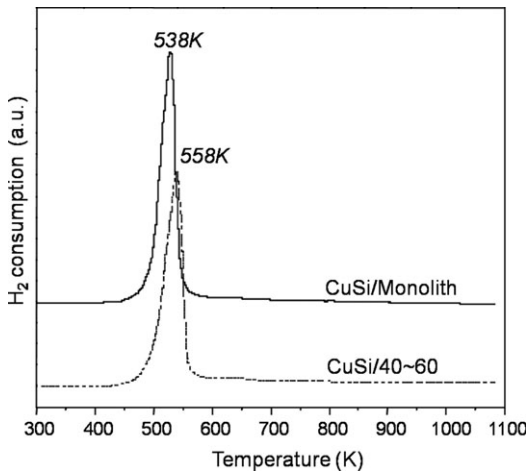

Figure 5. Temperature programmed reduction profiles of catalysts: CuSi/monolith (solid line) and CuSi/40–60 (dashed line).

Figure 6 showed XRD patterns of calcined and reduced CuSi/monolith and CuSi/40–60 samples. It has been reported that diffractions peaks at 35.4 and 38.7° correspond to CuO (tenorite), and the feature at 21.8° can be ascribed to silica.[7] For both calcined catalysts shown in Figure 6A, diffraction peaks for copper species were not observed, indicating that Cu was highly dispersed on SiO_2 and/or in an amorphous nature.[15] Clearly, the comparison also reveals the morphology of copper phyllosilicate in the wash-coat keep intact upon the ball-milling process.[59,60] For XRD patterns of the reduced catalysts (Figure 6B), strong diffraction peaks around 35.8° ascribable to the $Cu_2O(111)$ plane (JCPDS 05-

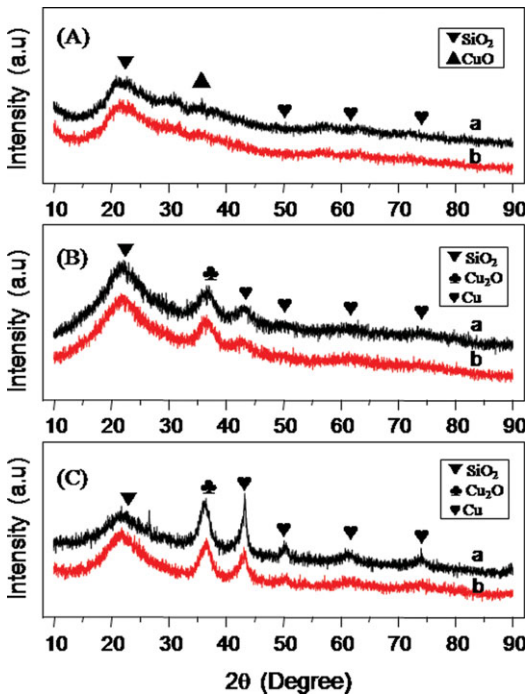

Figure 6. XRD patterns of the (A) calcined, (B) reduced and (C) used (a) CuSi/monolith and (b) CuSi/40–60 catalysts.

[Color figure can be viewed in the online issue, which is available at wileyonlinelibrary.com.]

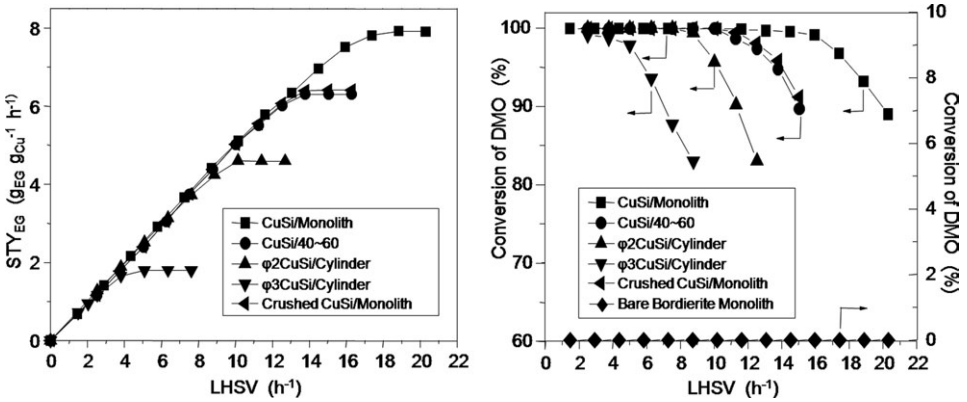

Figure 7. STY$_{EG}$ and conversion of DMO as a function of LHSV: (■) CuSi/Monolith, (◀) bed of CuSi/monolith crushed to particles smaller than 200 um, (●) bed of CuSi/40–60 particles smaller than 200 um, (▲) ϕ2CuSi/Cylinder catalyst, (▼) ϕ3CuSi/Cylinder catalyst, (◆) bare cordierite monolith with identical shape as CuSi/monolith.

Reaction conditions: P = 2.5 MPa, T = 473 K H_2/DMO = 80 mol/mol.

0667), while the diffraction peaks at 43.3°, 50.4°, and 74.1° are characteristic of Cu species (JCPDS 04-0836).[7] No CuO species observed on the both samples suggests that CuO was completely reduced to Cu_2O and Cu^0 or highly dispersed in silica.[7,15] The corresponding particle sizes of about 36 Å for Cu_2O and 24 Å for Cu were estimated based on the Scherrer equation. Comparatively, XRD patterns of the used catalysts, as shown in Figure 6C, are fairly different. Both the Cu_2O and Cu peaks of CuSi/40–60 catalyst are stronger than those of the CuSi/monolith, indicating that the crystal particle sizes of Cu (90 Å) and Cu_2O (51 Å) are larger compared to the used CuSi/monolith sample (49 Å for Cu and 42 Å for Cu_2O). This result agrees with the observation based on TEM characterization. It further suggests that the CuSi/monolith catalyst could slow the migration and inhibit sintering of Cu_2O and Cu particles under reaction and thermal treatment conditions.

Catalytic activities

Vapor-phase hydrogenation of DMO comprised several continuous reactions, including DMO hydrogenation to MG, MG hydrogenation to EG, and deep hydrogenation of EG to ethanol.[15] Moreover, byproducts of 1, 2-butanediol (1, 2-BDO) and 1, 2-propanediol (1, 2-PDO) could also be generated from the dehydrogenation reaction between EG and ethanol or methanol.[43,61]

Blank experiments showed that bare cordierite monolith was not active for the reaction. Comparing CuSi/monolith catalyst with that of the same catalyst smashed to pellets (250–350 μm), the former outperforms the packed bed in all the space velocity ranges (in Figure 7). Additionally, the CuSi/monolith catalyst also outperformed CuSi/40–60, achieving the highest total space time yield STY$_{EG}$ of 8.0 $g_{EG}\cdot g_{Cu}^{-1}\cdot h^{-1}$ (Table 2). The lower maximum STY$_{EG}$ for the CuSi/40–60 could be attributed to the internal diffusion limitation.[38] Additionally, lower conversion and selectivity of ϕ2CuSi/cylinder and ϕ3CuSi/cylinder catalysts could be also attributed to the internal diffusion limitations. Internal diffusion could become rate-limiting at high-space velocity for the ϕ2CuSi/cylinder and ϕ3CuSi/cylinder catalysts, which have a longer diffusion path vs. the CuSi/monolith. The longer diffusion path leads to the calculated values of $\eta\phi^2$ for DMO, EG and MG greater than 0.1 (discussed later in section of mass-transfer calculation). DMO conversion and STY$_{EG}$ for the crushed CuSi/monolith catalyst were comparable to the CuSi/40–60 but lower than CuSi/monolith catalyst, which indicates that the monolithic structure could enhance the catalytic activity effectively. More importantly, the highest EG selectivity was obtained on the CuSi/monolith catalyst, which would be an advantage for industrial production.

Effect of wash-coat thickness

Since the thickness of the wash-coat layer is a crucial factor for the internal mass transfer of monolith,[62,63] and could control the total reaction rate,[64] the monolithic catalysts with different wash-coat thickness were investigated. As shown in Table 3, the trend of DMO conversion and EG selectivity first increased with an increase of wash-coat thickness at the LHSV of 16 h^{-1}, and then decrease when the wash-coat

Table 2. Catalytic Performance for Hydrogenation of DMO to EG over CuSi/Monolith, CuSi/40–60 and Cylindrical Catalysts

			Conversion (%)	Selectivity (%)			
Catalysts	STY$_{EG}$[b] g_{EG} g_{cu}^{-1} h^{-1}	LHSV[c] h^{-1}	DMO	EG	MG	Ethanol	1,2-BDO
CuSi/40~60	6.3	13.7	95.4	92.8	5.1	1.1	0.9
ϕ2CuSi/Cylinder	4.6	10.2	94.2	91.9	4.5	1.9	1.7
Φ3CuSi/Cylinder	2.6	6.3	93.8	83.4	12.0	3.3	1.9
CuSi/Monolith	8.0	16.0[c]	99.6	95.3	3.0	0.9	0.8

[a] Reaction conditions: T = 473 K, P = 2.5 MPa, H_2/DMO = 80.
[b] STY$_{EG}$ represents the space time yield of EG, grams of EG per gram copper of catalyst per h.
[c] For the comparison with bed packed catalysts, the calculations of LHSV based on the weight of copper on the CuSi/monolith catalyst (35 μm thickness, 7.0 wt % Cu).

Table 3. Catalytic Performance and Calculated Wheeler-Weisz Group of Reactants and Products on the Monolithic Catalysts with Different Wash-Coat Thickness

	Wash-coat Thickness (μm)	Reactant		Product			
		H_2	DMO	EG	MG	Et	1,2-BDO
Wheeler-Weisz Value $\eta\phi^2$	7	1.0×10^{-4}	3.1×10^{-3}	2.3×10^{-3}	2.7×10^{-3}	1.0×10^{-4}	1.0×10^{-4}
	21	1.0×10^{-3}	2.8×10^{-2}	2.1×10^{-2}	2.5×10^{-2}	2.0×10^{-4}	3.0×10^{-4}
	28	1.8×10^{-3}	5.0×10^{-2}	3.7×10^{-2}	4.4×10^{-2}	3.0×10^{-4}	4.0×10^{-4}
	35	2.9×10^{-3}	7.8×10^{-2}	5.7×10^{-2}	6.9×10^{-2}	5.0×10^{-4}	6.0×10^{-4}
	40	3.7×10^{-3}	1.0×10^{-1}	7.4×10^{-2}	9.0×10^{-2}	6.0×10^{-4}	7.0×10^{-4}
Selectivity and Conversion (%)	7	–	78.1	74.7	24.2	0.3	0.4
	21	–	96.4	81.9	17.1	0.4	0.5
	28	–	99.0	90.5	8.0	0.6	0.7
	35	–	99.6	95.3	3.0	0.9	0.8
	40	–	99.4	94.7	2.7	1.3	1.1

[a] Condition: P = 2.5 MPa, T = 473 K, H_2/DMO = 80 mol/mol, LHSV = 16 h^{-1}.

thickness was higher than 35 μm. The yield of EG (in Figure 8) at LHSV of 16 h^{-1} was linearly increased with an increase in the wash-coat thickness and almost in parallel with the Cu mass concentration for the thickness lower than 40 μm. The slight difference may contribute to the concentration gradient in the wash-coat when the thickness was 10–150 μm.[63] The results indicate that the copper mass concentration contributed to the conversion of DMO and yield of EG. The decrease in activity is probably due to the internal mass-transfer limitation when the wash-coat thickness exceeded 35 μm. Therefore, under investigated condition, the optimal wash-coat thickness was about 35 μm.

Stability test

Stability and heat resistance test was performed over reduced CuSi/monolith and CuSi/40–60 catalysts at 473 K with a DMO LHSV of 10 h^{-1} and a H_2/DMO ratio of 80 (in Figure 9). Both catalysts demonstrated good stability since DMO conversion remained at 100% and selectivity of EG at 95% in the first test of 96 h. However, the catalytic performance under identical reaction conditions for CuSi/monolith and CuSi/40–60 catalysts after thermal treatment at 623 K for 24 h was significantly different. The initial DMO conversion (ca. 86%) and EG selectivity (ca. 83%) of the CuSi/40–60 catalyst were obtained, lower than those of the CuSi/monolith (90% DMO conversion and 86% EG selectivity). After 160 h, the DMO conversion was declined obviously, followed by a decrease in EG selectivity. In contrast, the thermal stability was notably enhanced over the CuSi/monolith catalyst, which demonstrated stable DMO conversion and EG selectivity for ~120 h before deactivation. Moreover, we notice that the shape of CuSi/monolith is almost as perfect as the fresh one after long-term test and heat treatment.

Mass-transfer calculation

As shown in Table 4, the Carberry numbers of all the reactants and products are much smaller than 0.05, which indicates that the mass transfer of the reactants from the gas bubbles to the catalyst surface has a negligible influence on the reaction. Theoretically, the flow profile will be fully developed before entering the catalyst bed in our reactor. The flow development length (L_d), calculated using the hydraulic diameter (D_h) and the Reynolds number (Re),[65,66] is found to be very short (ca. 40–60 mm), which is much smaller than distance (200 mm) between the flow entrance and top of the catalyst bed. Therefore, the fully developed flow will be beneficial for the external mass transfer in the catalyst bed.

In a heterogeneous catalytic system, internal mass-transfer resistance results from the diffusion of molecules within the porous materials. However, the film thickness in the square channels is hard to calculate accurately.[67,68] Therefore, the thin catalyst layer used in this work was approximate to be a porous slab.

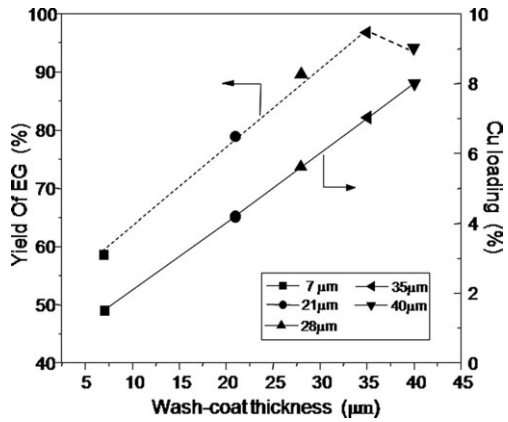

Figure 8. Yields of EG and Cu loading with different layer thickness of CuSi/monolith.

Reaction conditions: P = 2.5 MPa, T = 473 K H_2/DMO = 80 mol/mol, LHSV = 16 h^{-1}.

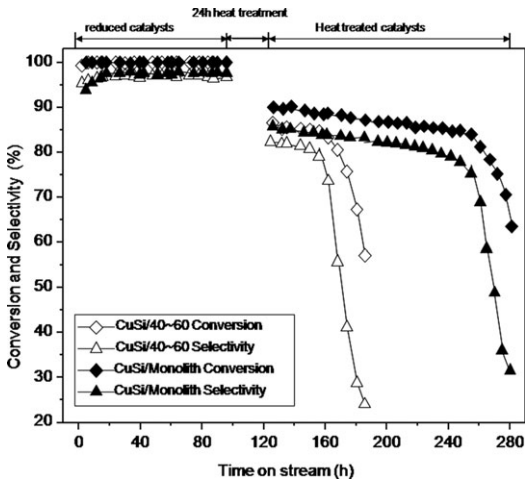

Figure 9. Stability tests with CuSi/monolith and CuSi/40–60 catalysts.

Table 4. Calculated Wheeler-Weisz Group and Observed Reaction Rate for Reactants and Products on CuSi/Monolith, CuSi/40–60 and Cylindrical Catalysts

		Reactant		Product			
catalysts		H_2	DMO	EG	MG	Ethanol	1,2-BDO
CuSi/Monolith	r_{obs} (mol s^{-1} g^{-1})	3.9×10^{-3}	1.9×10^{-3}	1.8×10^{-3}	1.9×10^{-3}	2.6×10^{-5}	2.3×10^{-5}
	$\eta\phi^2$	2.9×10^{-3}	7.8×10^{-2}	5.7×10^{-2}	6.9×10^{-2}	5.0×10^{-4}	7.0×10^{-4}
	Ca	7.1×10^{-5}	1.5×10^{-3}	1.3×10^{-3}	9.2×10^{-4}	3.1×10^{-4}	2.5×10^{-4}
CuSi/40∼60	r_{obs} (mol s^{-1} g^{-1})	3.6×10^{-3}	1.9×10^{-3}	1.8×10^{-3}	1.81×10^{-3}	2.4×10^{-5}	2.2×10^{-5}
	$\eta\phi^2$	8.1×10^{-3}	3.2×10^{-1}	3.0×10^{-1}	2.7×10^{-1}	1.7×10^{-3}	2.9×10^{-3}
	Ca	3.6×10^{-4}	2.4×10^{-3}	2.0×10^{-3}	1.4×10^{-3}	5.1×10^{-4}	3.9×10^{-4}
ϕ2CuSi/Cylinder	r_{obs}(mol s^{-1} g^{-1})	2.8×10^{-3}	1.4×10^{-3}	1.3×10^{-3}	1.3×10^{-3}	1.8×10^{-5}	2.6×10^{-5}
	$\eta\phi^2$	3.9×10^{-1}	1.1×10^{1}	8.8	9.4	6.4×10^{-2}	8.3×10^{-2}
	Ca	9.4×10^{-5}	7.5×10^{-3}	8.1×10^{-3}	6.1×10^{-3}	2.0×10^{-3}	1.1×10^{-3}
ϕ3CuSi/Cylinder	r_{obs} (mol s^{-1} g^{-1})	1.5×10^{-3}	7.5×10^{-4}	6.4×10^{-4}	6.7×10^{-4}	1.0×10^{-5}	1.3×10^{-5}
	$\eta\phi^2$	8.6×10^{-1}	2.4×10^{1}	1.9×10^{1}	2.1×10^{1}	1.2×10^{-1}	1.6×10^{-1}
	Ca	1.3×10^{-4}	3.6×10^{-3}	7.4×10^{-3}	5.3×10^{-3}	1.6×10^{-3}	8.9×10^{-4}

[a] Reaction condition: P = 2.5 MPa, T = 473 K, H_2/DMO = 80 mol/mol.

The calculated values for mass transfer over the monolithic catalysts with different thickness are listed in Table 3. It is noteworthy that the W-W value ($\eta\phi^2$) for the reactants on the CuSi/monolith are all significantly lower than 0.1, implying the internal mass transfer is negligible. It agrees with the results reported by Oh et al.,[54] and Hayes et al.[52,69] that the molecular diffusion in the wash-coat does not affect the reaction rate, when the thickness is lower than 50 μm. In our case, the wash-coat thickness of the monolith is within this range. However, the calculated W-W value of CuSi/monolith catalyst with 40 μm thickness of wash-coated is 0.102, slightly greater than the critical value 0.1, which indicates the effect of mass transfer on the reaction rate would not be negligible. It is in accordance with the results of catalytic activities tests shown in Table 3 and Figure 8 that the conversion of DMO and STY_{EG} of monolithic catalyst with thickness of 40 μm is lower than that of 35 μm.

On the other hand, the calculated W-W value of DMO, EG, and MG for the CuSi/40–60, ϕ2CuSi/cylinder, and ϕ3CuSi/Cylinder catalysts are all greater than 0.1, implying that the internal mass transfer influences the reaction rate in different degrees. Apparently, the $\eta\phi^2$ for the cylinder catalysts are significantly greater than 0.1; thus, internal mass-transfer resistances could be the main reason for their lower activity. Therefore, the calculated results proved that using the monolithic catalyst could effectively reduce the limitation of internal mass transfer and guarantee the hydrogenation of DMO in the kinetic region under these conditions.

Discussion

Reactivity and mass transfer

The originality of the higher conversion and STY_{EG} over the monolithic catalyst compared to the packed bed are not fully understood. Improved efficiency for mass transfer is crucial to obtain higher conversion and STY_{EG}. Therefore, several advantages of monolithic catalyst could account for the better performance, such as the better flow distribution, shorter diffusion pathway, and higher efficient utilization of the active phase.

Uniform distribution of flow in a multiphase reactor is important for enhancing conversion and STY[37] because of no catalyst bypassed by the gas and less dead zones, which are more likely to occur in packed beds.[70] The distribution of gas phase, studied in detail by using various techniques,[37,71] are general uniform inside monoliths. Once the uniform gas (distributed by gas distributor) enters the monolith channels, there is no further redistribution occurring inside.[37] A uniform flow distribution avoids detouring flow and dead zones, and ensures efficient utilization of the catalyst in the monolith,[36] and thus improves the conversion of DMO and STY_{EG}.

The nature of diffusion pathway suggested by The Weisz-Weisz modulus is a dominate factor accounting for the different catalytic performances between monolith and packed bed systems. The Wheeler-Weisz group based on a combination of effectiveness factor and the Thiele modulus does not represent accurately the results, although it would provides an estimate of the extent of wash-coat diffusion limitations.[40] Shorter diffusion paths in the monolith wash-coat induce the reactants and formed EG diffusing through the porous of wash-coat more readily from the catalytic sites and back into the gas phase.[35,36] Indeed, this hypothesis is supported by the different trends of DMO conversion and STY_{EG} between monoliths and packed beds (shown in Table 4 and Figure 7). The DMO conversions and STY_{EG} over monolith and packed beds are comparable in low-space velocity ranges, where smaller amount of produced EG are obtained. When the space velocity and the product of EG per unit volume increase, the inhibition by EG and other products involved is more relevant and, hence, the difference of conversion between monolith and fixed beds is more apparent. Even for the CuSi/40–60 sample, the surface layer of Cu-containing species is probably still too thick to be fully used compared to that in the wash-coat layer. It leads to the calculated $\eta\phi^2$ of DMO (0.32) and EG (0.30) over CuSi/40–60 pellects are much higher than that on CuSi/monolith and higher than the limit value of 0.1. Likewise, for both the ϕ2CuSi/cylinder and ϕ3CuSi/cylinder catalysts (with calculated $\eta\phi^2$ for DMO of 10.52 and 23.69, respectively), diffusion paths are comparably longer and the inhibiting effect of reactants and products increased signally, resulting in a small diffusivity. Furthermore, because of greater diffusive resistance, formed EG is more difficult to diffuse out from the active sites, thus, it was deeply hydrogenated to ethanol and 1, 2-butanediol.[7,15,72] It has shown that the reaction rate of the cylindrical catalysts is seriously limited by the internal mass transfer and, thus, the conversion and STY_{EG} are much lower.

Stability

Copper-based catalysts are extensively studied due to their excellent catalytic performance in many reactions. However, poor lifespan and thermal stability are the major drawbacks

for silica supported copper catalysts because they are significantly deactivated by sintering.[15,73–76] A way to estimate onset sintering temperature is based on the Tamman and Hüttig temperature,[77] where T_{Tamman} is the temperature at which atoms in the bulk will start to diffuse and $T_{\text{Hüttig}}$ is that when atoms at defects will become mobile. Both temperatures can be approximated by the following semiempirical equation: $T_{\text{Tamman}} = 0.5 \times T_{\text{melting}}$ and $T_{\text{Hüttig}} = 0.3 \times T_{\text{melting}}$. At the reaction conditions used in this work, the reaction temperature for attaining 100% conversion of DMO is 473 K, which is higher than the Hüttig temperature of Cu ($T_{\text{Melting,Cu}} = 1356$ K; $T_{\text{Melting,Cu2O}} = 1508$ K; $T_{\text{Hütting,Cu}} = 407$ K; $T_{\text{Hütting,Cu2O}} = 452$ K) but lower than the Tamman temperature ($T_{\text{Tamman,Cu}} = 678$ K; $T_{\text{Tamman,Cu}}O = 754$ K). Hydrogenation of DMO is a highly exothermic reaction system. From the thermodynamic analysis of main reactions, the ΔH_r of the overall reaction is 58.7 kJ/mol. The corresponding adiabatic temperature (ΔT) at the 473 K is about 35–56 K at the different reaction LHSV. Therefore, it would be a significant challenge to enhance thermal stability of the catalysts.

Stability tests for the CuSi/monolith and CuSi/40–60 catalysts shown in Figure 9 indicated that the stability of the CuSi/monolith is superior to that of the CuSi/40–60 catalyst, especially after the high-temperature treatment. Generally, uniform flow distribution could accelerate the heat dispersed evenly in a monolith reactor,[37] particularly in an exothermic reaction. Monolith structure is essentially a single structure with thin, vertical, parallel channels, separated from each other by walls.[37] In addition, the monolith could provide a regular channel structure for wash-coating catalyst, which favors the removal of reaction heat and consequently prevents the Cu nanoparticles from migrating and sintering. Moreover, it has been reported that the interaction between Cu and silica can be enhanced by forming copper phyllosilicate ($Cu_2Si_2O_5(OH)_2$), also called chrysocolla.[59] For the CuSi/monolith catalyst, the copper species in the chrysocolla were dispersed not only by SiO_2 but also the separated walls of cordierite, which may reduce the possibility of aggregation of Cu species during reaction after the high-temperature heat treatment. Additionally, the faster heat transfer would increase the selectivity of EG, whereas a high selectivity of byproducts (MG, ET, 1, 2-BDO) could be resulted at the higher temperature.

From the compared XRD patterns (Figure 6), the particle sizes of Cu grew up from 24 Å to 49 Å and of Cu_2O from 36 to 42 Å for CuSi/monolith catalyst upon usage, while Cu from 26 Å to 90 Å and Cu_2O from 39 to 51 Å for the CuSi/40–60 catalyst. Apparently, Cu particles grew more readily than Cu_2O due to the lower Tamman and Hüttig temperatures for Cu compared to Cu_2O. Indeed, the similar tendency of sintering was also observed on TEM images (Figure 3). He et al.,[15] and Yin et al.[78] reported that a oscillation of the copper chemical state runs through the course of the DMO catalytic hydrogenation. The Cu^0 species on the catalyst surfaces under working conditions may be oxidized to Cu^+ (the oxidation state +2 could also be occasionally reached) via the carbonyl oxygen atoms of the substrates (DMO, MG), and then reduced back to Cu^0 by hydrogen or active hydrogen species present on the surface.[15] For highly dispersed Cu-SiO_2 in the cordierite, the unique structure and uniform flow distribution of the CuSi/monolith system could play an important role in stabilizing small copper particles during the frequency of copper valence transition and then significantly retarding the growth of copper particles. Therefore, we could conclude that the CuSi/monolith could eventually mitigate the sintering of Cu and Cu_2O nanoparticles.

It is worth noting that the radial thermal transmission is a serious issue inside the monolith, since the channels are separated by the channel walls no radial mixing occurs.[37] Nevertheless, this defect can be solved by increasing the height-diameter ratio and gas-space velocity because of lower pressure drop in the monoliths.

Conclusions

We have presented an investigation regarding the hydrogenation of DMO to EG in a structured catalytic reactor consisting of Cu supported on silica-coated monoliths. The CuSi/monolith catalyst possesses not only the morphology of copper phyllosilicate, but also a regular channel structure, which makes the copper highly dispersed and remained anchored within the silica matrix. These features render the catalyst with high activity and stability for the reaction of hydrogenation of DMO, achieving a 100% conversion of DMO and 95% selectivity of EG. In comparison with packed bed of Cu/SiO_2, CuSi/monolith exhibits substantially higher conversion and STY_{EG}, with lower pressure drop that are attractive for industrial applications. We also presented evidence indicating that the mass-transfer resistances could be solved in the engineering scaling up, because the mass transfer could negligible over CuSi/monolith catalysts. Stability test of the CuSi/monolith catalyst showed excellent catalytic performance at the reaction temperature and heat resistance at the 623 K. This work illustrates that the monolithic catalyst could be an excellent candidate for production of EG via hydrogenation of DMO in practice.

Acknowledgments

We are grateful to the financial support from the China Postdoctoral Science Foundation (20090450090), Seed Foundation of Tianjin University (60303002), the Program for New Century Excellent Talents in University, and the Program of Introducing Talents of Discipline to Universities (B06006).

Notation

$\eta\phi^2$ = Weeler-Weisz group, dimensionless
r_{obs} = apparent reaction rate, mol L^{-1} s^{-1}
R = thickness of wash-coat or diameter of the pellet and cylindrical catalysts, m
u = the linear velocity through catalyst bed, m s^{-1}
Re = Reynolds numbers
Sh = Sherwood number
Sc = Schmidt number
J_D = Colburn J factor
D_h = hydraulic diameter, m
L_d = the flow development length (m), $L_d = 0.03 D_h Re$
ΔT = corresponding adiabatic temperature, K
$D_{eff,i}$ = effective diffusion coefficient in the pores of the catalyst, m^2 s^{-1}
C_i^* = concentration of specie i at the bulk of catalyst bed, mol m^{-3}
D_p = the diffusion coefficient in the pores, m^2 s^{-1}
D_K = the Knudsen diffusion coefficient, m^2 s^{-1}
$D_{B,i}$ = the bulk diffusion coefficient of specie i, m^2 s^{-1}
d_p = pore diameter of the catalyst, m
T = reaction temperature, K
M_i = the molar mass of the diffusing specie i, kg/mol
y_i = the molar percentage of the diffusing specie i, dimensionless
$D_{i,j}$ = binary diffusion coefficient, m^2 s^{-1}
P = reaction pressure, pa
V_i = the mean free path of the diffusing specie i, nm
W = catalyst weight, kg
V_r = catalyst volume, m^3
i = species, i = H_2, DMO, EG, MG, Ethanol, 1, 2-BDO

Greek letters

ϵ = porosity of porous medium, dimensionless
θ = void fraction (porosity) of catalyst bed, dimensionless
τ = tortuosity factor, dimensionless
ρ_g = gas density, kg m^{-3}
μ = molecular viscosity, kg m^{-1} s^{-1}

Literature Cited

1. Xu G, Li Y, Li Z, Wang H. Kinetics of the Hydrogenation of Diethyl Oxalate to Ethylene Glycol. *Ind Eng Chem Res*. 1995;34:2371–2378.
2. Cortright RD, Davda RR, Dumesic JA. Hydrogen from catalytic reforming of biomass-derived hydrocarbons in liquid water. *Nature*. 2002;418:964–967.
3. Liu J, Sun B, Hu JY, Pei Y, Li HX, Qiao MH. Aqueous-phase reforming of ethylene glycol to hydrogen on Pd/Fe3O4 catalyst prepared by co-precipitation: Metal-support interaction and excellent intrinsic activity. *J Catal*. 2010;274:287–295.
4. Huber GW, Shabaker JW, Dumesic JA. Raney Ni-Sn catalyst for H-2 production from biomass-derived hydrocarbons. *Science*. 2003; 300:2075–2077.
5. Bianchini C, Shen PK. Palladium-based electrocatalysts for alcohol oxidation in half cells and in direct alcohol fuel cells. *Chem Rev*. 2009;109:4183–4206.
6. Celik FE, Lawrence H, Bell AT. Synthesis of precursors to ethylene glycol from formaldehyde and methyl formate catalyzed by heteropoly acids. *J Mol Catal a-Chem*. 2008;288:87–96.
7. Chen LF, Guo PJ, Qiao MH et al. CU/SiO2 catalysts prepared by the ammonia-evaporation method: Texture, structure, and catalytic performance in hydrogenation of dimethyl oxalate to ethylene glycol. *J Catal*. 2008;257:172–180.
8. Gao ZH, Liu ZC, He F, Xu GH. Combined XPS and in situ DRIRS study of mechanism of Pd-Fe/alpha-Al2O3 catalyzed CO coupling reaction to diethyl oxalate. *J Mol Catal a-Chem*. 2005;235:143–149.
9. Jiang XZ, Su YH, Lee BJ, Chien SH. A study on the synthesis of diethyl oxalate over Pd/alpha-Al2O3 catalysts. *Appl Catal a-Gen*. 2001;211:47–51.
10. Teunissen HT, Elsevier CJ. Ruthenium catalysed hydrogenation of dimethyl oxalate to ethylene glycol. *Chem Commun*. 1997;1:667–668.
11. Boardman B, Hanton MJ, van Rensburg H, Tooze RP. A tripodal sulfur ligand for the selective ruthenium-catalysed hydrogenation of dimethyl oxalate. *Chem Commun*. 2006:2289–2291.
12. Teunissen HT. Homogeneous ruthenium catalyzed hydrogenation of esters to alcohols[double dagger]. *Chem Commun*. 1998:1367–1368.
13. Yin AY, Guo XY, Dai WL, Fan KN. High activity and selectivity of Ag/SiO2 catalyst for hydrogenation of dimethyl oxalate. *Chem Commun*. 2010;46:4348–4350.
14. Yin AY, Guo XY, Dai WL, Li HX, Fan KN. Highly active and selective copper-containing HMS catalyst in the hydrogenation of dimethyl oxalate to ethylene glycol. *Appl Catal a-Gen*. 2008;349:91–99.
15. He Z, Lin HQ, He P, Yuan YZ. Effect of boric oxide doping on the stability and activity of a Cu-SiO2 catalyst for vapor-phase hydrogenation of dimethyl oxalate to ethylene glycol. *J Catal*. 2011;277:54–63.
16. Yin AY, Guo XY, Dai WL, Fan KN. The nature of active copper species in cu-hms catalyst for hydrogenation of dimethyl oxalate to ethylene glycol: new insights on the synergetic effect between Cu-0 and Cu+. *J Phys Chem C*. 2009;113:11003–11013.
17. Yin AY, Guo XY, Fan KN, Dai WL. Ion-exchange temperature effect on cu/hms catalysts for the hydrogenation of dimethyl oxalate to ethylene glycol. *Chemcatchem*. 2010;2:206–213.
18. Brands DS, Poels EK, Bliek A. Ester hydrogenolysis over promoted Cu/SiO2 catalysts. *Appl Catal a-Gen*. 1999;184:279–289.
19. Sodesawa T, Nagacho M, Onodera A, Nozaki F. Dehydrogenation of methanol to methyl formate over Cu-SiO2 catatysts prepared by ion exchange method. *J Catal*. 1986;102:460–463
20. Kobayashi H, Takezawa N, Minochi C. Methanol reforming reaction over copper-containing catalysts The effects of anions and copper loading in the preparation of the catalysts by kneading method. *J Catal*. 1981;69:487–494
21. Haruhiko M, Kouichi H, Taizou U, Yasuo N, Seizou I, Takanori T, Inventors. US patent 57122946. 1982.
22. Kouichi H, Taizou U, Yasuo N, Inventors. US patent 4614728. 1986.
23. Miyazaki H, Uda T, Hirai K, Nakamura Y, Ikezawa H, Tsuchie T, Inventors. Process for producing ethylene glycol and/or glycolic acid ester, catalyst composition used therefore, and process for production. US patent 4585890. 1986.
24. Yin AY, Guo XY, Fan KN, Dai WL. Influence of copper precursors on the structure evolution and catalytic performance of Cu/HMS catalysts in the hydrogenation of dimethyl oxalate to ethylene glycol. *Appl Catal a-Gen*. 2010;377:128–133.
25. Guo XY, Yin AY, Dai WL, Fan KN. One pot synthesis of ultrahigh copper contented Cu/SBA-15 material as excellent catalyst in the hydrogenation of dimethyl oxalate to ethylene glycol. *Catal Lett*. 2009;132:22–27.
26. Carlini C, Di Girolamo M, Macinai A et al. Selective synthesis of isobutanol by means of the Guerbet reaction Part 2. Reaction of methanol/ethanol and methanol/ethanol/n-propanol mixtures over copper based/MeONa catalytic systems. *J Mol Catal a-Chem* 2003;200:137–146.
27. Liu DS, Zhang JG, Li DF, Kong QD, Zhang T, Wang SD. Hydrogenation of 2-ethylanthraquinone under taylor flow in single square channel monolith reactors. *AIChE J*. 2009;55:726–736.
28. Ramanathan K, Gopinath A. Light-off location and front diffusion in a catalytic monolith reactor. *AIChE J*. 2008;54:1860–1873.
29. Joshi SY, Harold MP, Balakotaiah V. Low-dimensional models for real time simulations of catalytic monoliths. *AIChE J*. 2009;55:1771–1783.
30. Kapteijn F, Nijhuis TA, Heiszwolf JJ, Moulijn JA. New non-traditional multiphase catalytic reactors based on monolithic structures. *Catal Today*. 2001;66:133–144.
31. Centi G, Perathoner S. Novel catalyst design for multiphase reactions. *Catal Today*. 2003;79:3–13.
32. Williams JL. Monolith structures, materials, properties and uses. *Catal Today*. 2001;69:3–9.
33. Ramanathan K, Balakotaiah V, West DH. Ignition criterion for general kinetics in a catalytic monolith. *AIChE J*. 2006;52:1623–1629.
34. Al-Dahhan MH, Kemoun A, Cartolano AR. Phase distribution in an upflow monolith reactor using computed tomography. *AIChE J*. 2006;52:745–753.
35. Boger T, Heibel AK, Sorensen CM. Monolithic catalysts for the chemical industry. *Ind Eng Chem Res*. 2004;43:4602–4611.
36. Nijhuis TA, Beers AEW, Vergunst T, Hoek I, Kapteijn F, Moulijn JA. Preparation of monolithic catalysts. *Catal Rev*. 2001;43:345–380.
37. Roy S, Bauer T, Al-Dahhan M, Lehner P, Turek T. Monoliths as multiphase reactors: A review. *AIChE J*. 2004;50:2918–2938.
38. Wheeler A. *Advance in Catalysis*. Vol 3. New York: Academic Press; 1951.
39. Weisz PB, Prater DC. *Advances in Catalysis*. Vol 6. New York: Academic Press; 1954.
40. Zhang F, Hayes RE, Kolaczkowski ST. A new technique to measure the effective diffusivity in a catalytic monolith washcoat. *Chem Eng Res Des*. 2004;82:481–489.
41. Zhao YJ, Zhou J, Zhang JG, Li DY, Wang SD. Selective hydrogenation of benzene to cyclohexene on a Ru/Al2O3/cordierite monolithic catalyst: Effect of mass transfer on the catalytic performance. *Ind Eng Chem Res*. 2008;47:4641–4647.
42. Carniglia SC. Construction of the tortuosity factor from porosimetry. *J Catal*. 1986;102:401–418.
43. Van Der Grift CJG, Wielers AFH, Jogh BPJ et al. Effect of the reduction treatment on the structure and reactivity of silica-supported copper particles. *J Catal*. 1991;131:178–189.
44. Chinchen GC, Hay CM, Vandervell HD, Waugh KC. The measurement of copper surface areas by reactive frontal chromatography. *J Catal*. 1987;103:79–86.
45. Carberry JJ. *Physico-Chemical Aspects of Mass Transfer in Heterogeneous Catalysis*. Vol 8. Berlin: SpringerVerlag; 1987.
46. Ronchin L, Marziano NC, Tortato C, Vavasori A, Badetti C. Catalyzed Beckmann rearrangement of cyclohexanone oxime in heterogeneous liquid/solid system Part 1: Batch and continuous operation with supported acid catalysts. *J Mol Catal a-Chem*. 2007;277: 221–232.
47. Ronchin L, Toniolo L. Selective hydrogenation of benzene to cyclohexene catalyzed by Ru supported catalysts - Influence of the alkali promoters on kinetics, selectivity and yield. *Catal Today*. 2001;66: 363–369.
48. Carberry JJ. *Physico-Chemical Aspects of Mass Transfer in Heterogeneous Catalysis*. Vol 8. Berlin: SpringerVerlag; 1987.
49. Fogler HS. *Essentials of Chemical Reaction Engineering*. 3rd ed. New Jersey: Prentice-Hall International, Inc.; 2009.

50. Dwivedi PN, Upadhyay SN. Particle-fluid mass transfer in fixed and fluidized beds. *Ind Eng Chem Proc Des Develop*. 1977;16:157–165.
51. Venkatesan R, Fogler HS. Comments on analogies for correlated heat and mass transfer in turbulent flow. *AIChE J*. 2004;50: 1623–1626.
52. Arnby K, Törncrona A, Andersson B, Skoglundh M. Investigation of Pt/[gamma]-Al2O3 catalysts with locally high Pt concentrations for oxidation of CO at low temperatures. *J Catal*. 2004;221:252–261.
53. Ronchin L, Toniolo L. Selective hydrogenation of benzene to cyclohexene using a suspended Ru catalyst in a mechanically agitated tetraphase reactor. *Catal Today*. 1999;48:255–264.
54. Sudheesh N, Sharma SK, Khokhar MD, Shukla RS. Kinetic investigations on the modified chitosan catalyzed solvent-free synthesis of jasminaldehyde. *J Mol Catal A Chem*. 2011.In press.
55. Robert GW. *Catalysis in Organic Synthesis*. New York: Academic Press; 1976.
56. Ramachadran PA, Chaudhari RV. *Three-Phase Catalytic Reactors*. Gorden & Breach Science Publishers; 1982.
57. Froment GF, Bischoff KB. *Chemical Reactor Analysis and Design*. New York: Wiley; 1990.
58. Poling BE, Prausnitz JM, Connell JPO. *The Properties of Gases and Liquids*. New York: McGraw-Hill; 2001.
59. Toupance T, Kermarec M, Lambert JF, Louis C. Conditions of formation of copper phyllosilicates in silica-supported copper catalysts prepared by selective adsorption. *J Phys Chem B*. 2002;106:2277–2286.
60. Toupance T, Kermarec M, Louis C. Metal particle size in silica-supported copper catalysts. influence of the conditions of preparation and of thermal pretreatments. *J Phys Chem B*. 2000;104:965–972.
61. Van Der Grift CJG, Muldera A, Geusa JW. Preparation of silica-supported copper catalysts by means of deposition-precipitation *Appl Catal*. 1990;60:181–192
62. Hayes RE, Kolaczkowski ST. A study of Nusselt and Sherwood numbers in a monolith reactor. *Catal Today*. 1999;47:295–303.
63. Hayes RE, Kolaczkowski ST. Mass and heat transfer effects in catalytic monolith reactors. *Chem Eng Sci*. 1994;49:3587–3599.
64. Kolaczkowski ST. Modelling catalytic combustion in monolith reactors - challenges faced. *Catal Today*. 1999;47:209–218.
65. Bejhed J et al. Numerical modeling and verification of gas flow through a network of crossed narrow v-grooves. *J Micromech Microeng*. 2006;16:2006.
66. Gravesen P et al. Microfluidics-a review. *J Micromech Microeng*. 1993;3:168.
67. Nijhuis TA, Kreutzer MT, Romijn ACJ, Kapteijn F, Moulijn JA. Monolithic catalysts as efficient three-phase reactors. *Chem Eng Sci*. 2001;56:823–829.
68. Kreutzer MT, Bakker JJW, Kapteijn F, Moulijn JA, Verheijen PJT. Scaling-up multiphase monolith reactors: Linking residence time distribution and feed maldistribution. *Ind Eng Chem Res*. 2005;44:4898–4913.
69. Hayes RE, Liu B, Moxom R, Votsmeier M. The effect of washcoat geometry on mass transfer in monolith reactors. *Chem Eng Sci*. 2004;59:3169–3181.
70. Plana C, Armenise S, Monzon A, Garcia-Bordeje E. Ni on alumina-coated cordierite monoliths for in situ generation of CO-free H-2 from ammonia. *J Catal*. 2010;275:228–235.
71. Heibel AK, Vergeldt FJ, van As H. Gas and liquid distribution in the monolith film flow reactor. *AIChE J*. 2003;49:3007–3017.
72. Yin AY, Guo XY, Dai WL, Fan KN. Effect of initial precipitation temperature on the structural evolution and catalytic behavior of Cu/SiO2 catalyst in the hydrogenation of dimethyloxalate. *Catal Commun*. 2011;12:412–416.
73. Kam R, Selomulya C, Amal R, Scott J. The influence of La-doping on the activity and stability of Cu/ZnO catalyst for the low-temperature water-gas shift reaction. *J Catal*. 2010;273:73–81.
74. Chen CS, Cheng WH, Lin SS. Enhanced activity and stability of a Cu/SiO2 catalyst for the reverse water gas shift reaction by an iron promoter. *Chem Commun*. 2001:1770–1771.
75. Kameoka S, Tanabe T, Tsai AP. Spinel CuFe2O4: a precursor for copper catalyst with high thermal stability and activity. *Catal Lett*. 2005;100:89–93.
76. Chen CS, Cheng WH, Lin SS. Study of iron-promoted Cu/SiO2 catalyst on high temperature reverse water gas shift reaction. *Appl Catal a-Gen*. 2004;257:97–106.
77. Charles NS. *Heterogeneous Catalysis in Industrial Practice*. 2nd ed. New York: McGraw-Hill; 1996.
78. Yin A, Wen C, Guo X, Dai W-L, Fan K. Influence of Ni species on the structural evolution of Cu/SiO2 catalyst for the chemoselective hydrogenation of dimethyl oxalate. *J Catal*. 2011;280:77–88.

Manuscript received Jun. 14, 2011, and revision received Sept. 26, 2011.